Length Scales in the Convective Boundary Layer

DONALD H. LENSCHOW AND B. BOBA STANKOV*

*National Center for Atmospheric Research, Boulder, CO 80307***

(Manuscript received 11 July 1985, in final form 16 January 1986)

ABSTRACT

We calculated integral scales for horizontal and vertical velocity components, temperature, humidity and ozone concentration, as well as for their variances and covariances from aircraft measurements in the convective atmospheric boundary layer over both ocean and land surfaces. We found that the integral scales of the second-order moment quantities are 0.67 ± 0.09 that of the variables themselves. Consequently, only the second-order moment integral scales are presented here. These results are used to calculate the averaging lengths necessary to measure second-order moment quantities to a given accuracy. We found that a measurement length of 10 to 100 times the boundary-layer height is required to measure variances to 10% accuracy, while scalar fluxes require a measurement length of 10^2 to 10^4 and stress a measurement length of 10^3 to 10^5 times the boundary layer height. We also show that the ratio of the wavelength of the spectral peak to the integral scale can be used to estimate the sharpness of the spectral peak.

1. Introduction

An important consideration in observational studies of the atmospheric boundary layer is the length or time over which, on the average, a variable maintains some degree of correlation with itself. For fixed-point boundary layer observations, a time scale is often specified which can be related to a length scale by multiplying the mean wind speed by the time scale. This requires the assumption of "frozen turbulence" known as Taylor's hypothesis (Panofsky and Dutton, 1984). Alternatively, the measurement platform may itself be moving as, for example, an aircraft. Aircraft, however, typically fly an order of magnitude faster than the mean wind and thus Taylor's hypothesis is more easily fulfilled. Since we use airplane measurements here, we calculate length scales by multiplying the measured time scale by the true airspeed. The length scale is a useful concept for examining the structure of turbulent fields and how the structure is modified by the hydrodynamic stability, surface properties, height above the surface, and boundary-layer depth. It is also closely related to the maximum in the spectral density times wavenumber since the length scale is commonly defined in terms of the integral of the autocorrelation coefficient, which can be computed from the spectral density by a Fourier transformation.

In addition to its intrinsic value as a parameter describing a characteristic of a turbulent field, the length scale of a variable is used in conjunction with the standard deviation of a measurement to estimate the length over which a variable must be measured in order to obtain a specified accuracy. There have been many studies of accuracy of measurements based on intercomparisons with several sensors and on estimated accuracies of particular sensors, but relatively few studies that have dealt with the question of the length of measurement necessary to achieve a specified accuracy because of the variability and the scale of variability of the atmosphere. Lumley and Panofsky (1964) discuss this problem, and Wyngaard (1973, 1983a) presents more detailed analyses of required measurement lengths to achieve a specified accuracy of both mean and second-order moment quantities in the boundary layer. We are not aware of any study, however, that systematically estimates the integral length scale of variables in the convective boundary layer normalized by the boundary-layer height. In this paper we present results from aircraft flights for several second-order-moment variables, and show that the integral scale of a variable is only slightly larger than that for the square of the variable. Consequently the integral scale for second-order moments can also be used to estimate the integral scale for the variables themselves.

2. Theoretical background

When making turbulence observations in the atmospheric boundary layer, ideally we would like to be able to obtain ensemble averages of the turbulence statistics. However, such averages cannot be measured. Instead, averages over space (or time) are obtained, and assumed to be estimates of the ensemble average. A standard measure of the difference between the es-

* Present affiliation: NOAA/Wave Propagation Laboratory, Boulder, CO 80303.

** The National Center for Atmospheric Research is sponsored by the National Science Foundation.

© 1986 American Meteorological Society

Unauthenticated | Downloaded 10/05/24 05:53 AM UTC

timated average and the ensemble average for a homogeneous random function $f(x)$ is

$$\sigma_f^2 = \langle(\bar{f} - \langle f\rangle)^2\rangle, \tag{1}$$

where $\bar{f}$ and $\langle f\rangle$ are the space (or time) and ensemble averages, respectively.

The integral length scale is defined as

$$\lambda_f = \int_0^\infty R_f(r)dr/R_f(0), \tag{2}$$

with

$$R_f(r) = \langle f'(x)f'(x+r)\rangle, \tag{3}$$

where a prime denotes departures from the ensemble average of $f(x)$. The function $R_f(r)$ is the autocovariance function. Normalizing the autocovariance function by the variance $R_f(0) = \langle f'^2\rangle$ gives us the autocorrelation function $\rho_f(r)$. Assuming that the integral scale exists, it can be shown that for λ_f much smaller than the averaging length L_f (Lumley and Panofsky, 1964) the error variance is given by

$$\sigma_f^2 = \frac{2\langle f'^2\rangle\lambda_f}{L_f}. \tag{4}$$

If we specify an acceptable relative error $\sigma_f/\langle f\rangle = a$, the required averaging length becomes

$$L_f = \frac{2\langle f'^2\rangle\lambda_f}{\langle f\rangle^2 a^2}. \tag{5}$$

Let α and β denote measured variables with zero ensemble means. Then for $f = \alpha\beta$, (5) becomes

$$L_{\alpha\beta} = \frac{2(\langle\alpha^2\beta^2\rangle - \langle\alpha\beta\rangle^2)\lambda_{\alpha\beta}}{\langle\alpha\beta\rangle^2 a^2}. \tag{6}$$

Even-order moments of velocity and scalar variables are usually observed to be approximately Gaussian in a convective boundary layer (e.g., Wyngaard, 1983b). We assume that α and β are sufficiently close to being joint Gaussian that $\langle\alpha^2\beta^2\rangle = \langle\alpha^2\rangle\langle\beta^2\rangle + 2\langle\alpha\beta\rangle^2$. Then (6) becomes

$$L_{\alpha\beta} = 2(r_{\alpha\beta}^{-2} + 1)\lambda_{\alpha\beta}/a^2, \tag{7}$$

where the correlation coefficient $r_{\alpha\beta} \equiv \langle\alpha\beta\rangle/(\langle\alpha^2\rangle \times \langle\beta^2\rangle)^{1/2}$. As a special case for $\beta = \alpha$, i.e., for the variance of α, (6) reduces to

$$L_{\alpha^2} = \frac{2\lambda_{\alpha^2}}{a^2}(K_\alpha - 1), \tag{8}$$

where $K_\alpha \approx 3$ is the kurtosis of α. Thus, we have shown that (5) can also be used to specify the averaging necessary to obtain turbulence statistics to a specified accuracy.

3. Techniques of analysis

For each flight leg used in the subsequent analysis, the autocorrelation function was obtained by 1) removing a linear trend from the time series, 2) calculating the power spectral density with a Fast Fourier Transform algorithm, and 3) calculating the inverse Fourier transform of the spectral density. Figure 1 shows a typical autocorrelation function, as well as a plot of $F(r) = (\int_0^r R(r')dr')/R(0)$. The maximum value of $F(r)$ was then taken as the integral scale of the process (see Appendix A).

Wyngaard (1973, 1983a) discusses applications of (5), particularly to second-order moments, pointing out that there is more experimental scatter for the same averaging length in the mixed layer of the boundary layer than in the surface layer because of the larger integral scale and, for many covariances, the smaller correlation coefficient of the turbulence variables in the mixed layer. He found, for example, that some second-order moments may require averaging over distances of hundreds of kilometers to achieve 10% accuracy.

4. Description of data and calculations

We use data from several experiments involving aircraft flights in the convective boundary layer. The first of these was the Air Mass Transformation Experiment (AMTEX), e.g., Lenschow and Agee (1976), which was conducted over the East China Sea to study wintertime cold air advection over relatively warm water. Wyngaard et al. (1978), and Lenschow and Stephens (1980) further describe the instrumentation and weather conditions during the six NCAR Electa flights used here. The second was a series of flights over eastern Colorado in an NCAR Queen Air aircraft during September 1979. One objective was to study the vertical turbulent flux of ozone in the convective boundary layer (Lenschow et al., 1981). The third was a similar series of flights in an NCAR Queen Air aircraft during June 1980 over the Gulf of Mexico (Lenschow et al., 1982). The relevant mixed-layer scaling parameters and conditions for all the flights used here are listed in Table 1. Although clouds were present on some of the flights, we do not think that they significantly affected the length analyses. The clouds were stratocumulus, about a hundred meters or so thick beneath a capping inversion (in AMTEX), or a few scattered fair-weather trade cumuli (Gulf of Mexico), and seemed to have negligible dynamic effect on the boundary layer structure. The flights were conducted in relatively horizontally homogeneous situations, although this does not, of course, preclude contributions to the length scales due to mesoscale variability. For each flight, the sets of legs include along- and cross-wind traverses which were then averaged together before plotting. The data were available at a sample rate of 20 s^{-1}, and the airplane speed was 70 to 100 m s^{-1}.

For the AMTEX flights the number of legs inside the boundary layer varied between four and six. The shortest leg was 42 km long; the longest was 119 km. Flight 7 of the eastern Colorado flights had four legs

Unauthenticated | Downloaded 10/05/24 05:53 AM UTC

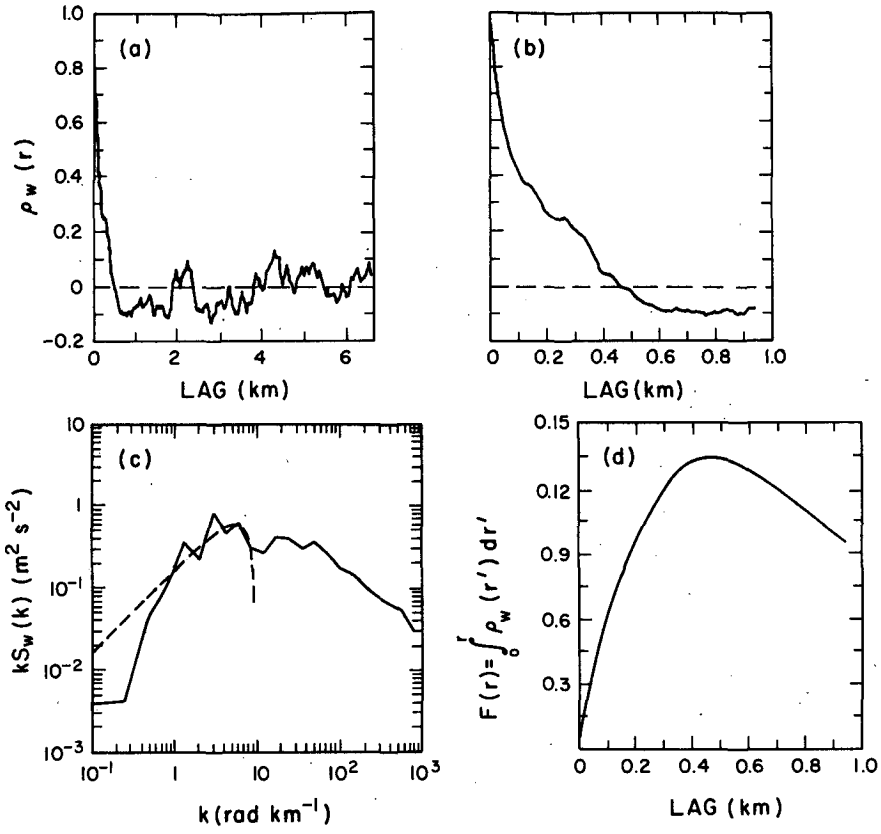

FIG. 1. A sample autocorrelation function for vertical velocity extending out to about 6.6 km, which shows the random fluctuations in the function beyond the lag to which correlation extends (a), and to about 0.94 km, which shows the detailed structure of the function in the domain where correlation exists (b). The power spectrum, which is the Fourier transform of the autocovariance function, is shown in (c); the dashed line is the function

$$S(k) = \frac{3\sigma_w^2}{4k_0}[1 - (k/k_0)^2].$$

Panel (d) is $F_w(r) = \int_0^r \rho_w(r')dr'$.

inside the boundary layer varying from 42 km to 84 km in length, and the Gulf of Mexico flight had three legs, each about 170 km long.

Integral and averaging length scales (for 10% measurement accuracy) were then calculated for u (eastward), v (northward), and w (vertical) wind components, potential temperature θ, absolute humidity q, and ozone concentration s, as well as the momentum, temperature, moisture, and ozone vertical fluxes and the covariances $\langle\theta's'\rangle$, $\langle\theta'q'\rangle$, and $\langle q's'\rangle$.

TABLE 1. Boundary-layer parameters for the airplane flights used here. L is the Monin-Obukhov length, u_* is the friction velocity, and the other parameters are defined in (9). All but the flights on 19 Sep 1979 were over the ocean. Ozone mixing ratio was measured only on the last two flights.

Date	Figure symbol	Wind speed and direction (m s^{-1}/deg)	T (air) (K)	z_i (m)	$-L$ (m)	u_* (m s^{-1})	w_* (m s^{-1})	T_* (K)	q_* (g m^{-3})	s_* (ppbv)
15 Feb 75	□	10/350	283–288	1200	76	.53	1.88	.073	.079	
16 Feb 75	▼	8/350	283–287	1430	40	.40	1.86	.060	.075	
18 Feb 75	●	8/350	289	1010	44	.35	1.41	.042	.099	
22 Feb 75	×	15/350	285	1900	67	.58	2.51	.079	.121	
24 Feb 75	○	8/140	289	1200	22	.30	1.61	.047	.126	
26 Feb 75	▲	9/60	291	680	59	.33	1.06	.037	.089	
19 Sep 79	★	6/190	294	860	114	.50	1.45	.072	.012	.131
12 Jun 80	△	6/80	299	1000	113	.27	0.81	.007	.080	.052

Unauthenticated | Downloaded 10/05/24 05:53 AM UTC

5. Results

a. Integral scales

In order to generalize the results from eight different flights, we used the following mixed-layer scaling parameters to normalize the variables:

$$\left.\begin{aligned} z_i &\equiv \text{height of boundary layer} \\ w_* &\equiv [(g/T\langle w'\theta_v'\rangle_0 z_i]^{1/3} \\ \theta_* &\equiv \langle w'\theta'\rangle_0/w_* \\ q_* &\equiv \langle w'q'\rangle_0/w_* \\ s_* &\equiv \langle w's'\rangle_0/w_* \end{aligned}\right\} \quad (9)$$

where θ_v is virtual potential temperature. The subscript zero denotes a surface layer value, and g/T is the buoyancy parameter.

We calculated integral scales for variables themselves, as well as their variances, and found the integral scales of the variables to be slightly larger than those for the variances, with a nearly constant value for their ratio. The mean and standard deviation of the ratio of the variance integral scale to the mean integral scale for all the variables considered here were 0.67 and 0.09, respectively. An example of the integral scales for the mean and variance of w and horizontal velocity v_H is shown in Fig. 2. In this example, the length scale λ_{vH} is defined as the average of the length scales for the along- and cross-wind legs. Lumley and Panofsky (1964) state that for a Gaussian process with a nonnegative correlation function, the integral scale of a process generated by taking a function of the original process is no larger than the integral scale of the original process. In Appendix B we show that this ratio is equal to 0.57 for a process with an autocorrelation function that is characteristic of turbulence in the inertial subrange, extended out to the zero crossing of the autocorrelation function.

Since measurements were obtained from both along- and cross-wind flight legs, we also investigated the asymmetry of the boundary-layer turbulence structure in the horizontal plane. Since the spectral calculations

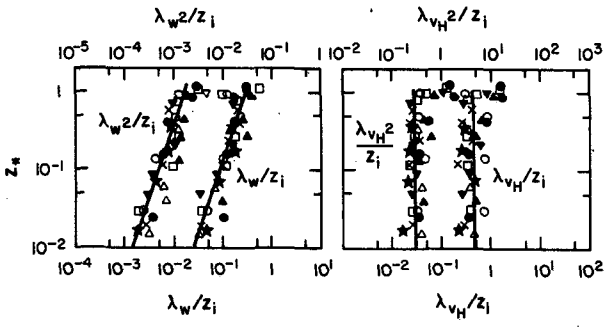

FIG. 2. Integral scales of w and v_H (lower scales) and w^2 and v_H^2 upper scales.

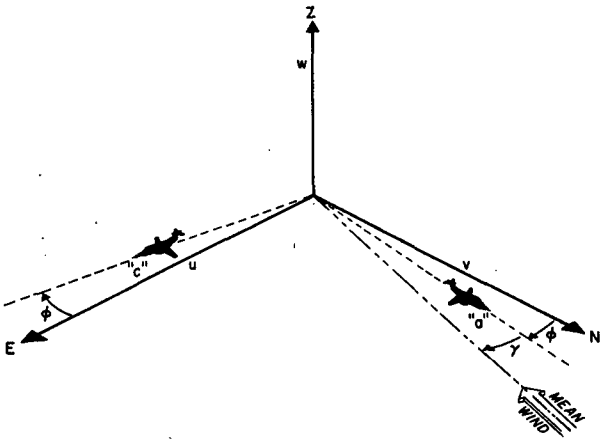

FIG. 3. Schematic showing the airplane heading ϕ and the angle of the mean wind with respect to the airplane γ. The angle of the mean wind $\gamma + \phi$ is measured in a geographic coordinate system where u and v are the west and south wind components, respectively.

for the horizontal velocity components were carried out on the wind components rotated to the N–S and E–W directions, a subset of flight legs was selected in which the wind direction [$(\gamma + \phi)$, where γ is the angle between the airplane along-wind heading and the mean wind direction, and ϕ is the along-wind aircraft heading] and ϕ were within 20° of the N–S axis (see Fig. 3). Four out of the eight sets of flight legs met this criteria. We then plotted the logarithm of the ratio of the along-wind to cross-wind integral scales of the variances for each of the selected sets of legs and calculated their means and standard deviations. The logarithms of the ratios were found to be normally distributed, which means that the distributions of the ratios are log normal. The significance of the means were then estimated using the Student-t distribution. There was no discernible variation of the ratios with height.

Let subscript a denote the along-wind flight direction, and c the cross-wind flight direction, as in Fig. 3. We note that because the mean wind for this subset of flight legs is within 20° of the N–S direction, the u, or east wind component, is very nearly the cross-wind component, and the v component the along-wind component. Batchelor (1953) shows that for isotropic turbulence the ratio of lateral to longitudinal integral scales for the horizontal velocity components is 0.5. Boundary layer turbulence is definitely not isotropic. We found that the mean for $\lambda_{au}/\lambda_{cu}$ was 1.0, with 90% confidence limits of 0.8 to 1.3, while the mean for $\lambda_{cv}/\lambda_{av}$ was 0.8 with 90% confidence limits of 0.7 and 1.0. Thus, the measured ratios of lateral to longitudinal integral scales for each of the two wind components gave a value closer to 1.0 than 0.5; in fact, on the basis of the two-sided t-test, we can reject the hypothesis that the measured ratio was 0.5, since the probability of either measured ratio being 0.5 was less than 0.001. The measured ratios of $\lambda_{au}/\lambda_{av}$ and $\lambda_{cv}/\lambda_{cu}$, which again

Unauthenticated | Downloaded 10/05/24 05:53 AM UTC

should be 0.5 for isotropic turbulence, were 1.1 and 0.7, respectively. Similar results were obtained for the measured ratios of $\lambda_{au^2}/\lambda_{cu^2}$, $\lambda_{cv^2}/\lambda_{av^2}$, $\lambda_{au^2}/\lambda_{av^2}$ and $\lambda_{cv^2}/\lambda_{cu^2}$.

We also calculated the ratios of the integral scales of the lateral components along- and cross-wind and the longitudinal components along- and cross-wind. In isotropic turbulence, these ratios should be unity. We found that the mean for $\lambda_{au}/\lambda_{cv}$ was 1.4 with 90% confidence limits of 1.1 and 1.8, while the mean for $\lambda_{cu}/\lambda_{av}$ was 1.2 with 90% confidence limit of 0.9 and 1.4. The hypothesis that $\lambda_{au}/\lambda_{cv}$ is unity has a probability of only 2.3%, so that it is quite probable that the ratio is actually greater than one. On the other hand, the ratios $\lambda_{au^2}\lambda_{cv^2}$ and $\lambda_{cu^2}/\lambda_{av^2}$ did not differ significantly from one at the 10% significance level. The measured ratios of the lateral to the longitudinal components of the vertical momentum flux behaved similarly to the wind components. We found that $\lambda_{auw}/\lambda_{cuw} = 1.0$ with 90% confidence limits of 0.8 to 1.3, while $\lambda_{cvw}/\lambda_{avw} = 0.8$ with 90% confidence limits of 0.6 to 0.9.

On the basis of these results, we did not further pursue the question of whether there may actually be some slight difference between along- and cross-wind integral scales for the horizontal velocity components, and instead averaged together the along- and cross-wind measurements of the integral scales for both $\langle u'^2\rangle$ and $\langle v'^2\rangle$, and both $\langle u'w'\rangle$ and $\langle v'w'\rangle$.

The measured ratio for the vertical wind component was $\lambda_{aw}/\lambda_{cw} = 1.7$, with 90% confidence limits of 1.4 and 2.0, and for the variance $\lambda_{aw^2}/\lambda_{cw^2} = 1.2$, with 90% confidence limits of 1.0 and 1.6. Similarly, the measured ratios for the vertical fluxes of temperature and water vapor were $\lambda_{aw\theta}/\lambda_{cw\theta} = 1.2$, with 90% confidence limit of 1.0 and 1.5, and $\lambda_{awq}/\lambda_{cwq} = 1.3$, with 90% confidence limits of 1.1 and 1.5. Therefore, we can conclude that the vertical wind component, as well as the eddies that transport heat and moisture, are elongated along the direction of the wind.

On the other hand, the measured integral scale ratios for θ, $\langle\theta'^2\rangle$, q and $\langle q'^2\rangle$, were all insignificantly different from one. Furthermore, looking separately at the integral scales of the along- and cross-wind legs for all the variables did not reduce the scatter in the results nor change their height dependency.

Integral length scales for the variances and covariances are shown in Figs. 4 and 5. All the results are averages of along- and cross-wind legs. Using the normalized height scale $z_* = z/z_i$, the integral length scales for the variances are well represented by

$$\left.\begin{aligned} \lambda_{w^2}/z_i &= 0.16z_*^{1/2} \\ \lambda_{v_H^2}/z_i &= \frac{\lambda_{u^2}+\lambda_{v^2}}{2z_i} = 0.30 \\ \lambda_{c_i^2}/z_i &= z_*^{1/2} \end{aligned}\right\} \qquad (10)$$

where the subscript c_i denotes potential temperature, humidity, and ozone concentration. Thus, we find that, with the exception of $\lambda_{v_H^2}$, the variance integral scales increase by about a factor of 8 from $z_* = 0.015$, which is about the lowest measurement level, to the top of the boundary layer, with λ_{w^2} being about one-sixth that of the scalar integral scales. On the other hand, $\lambda_{v_H^2}$ remains approximately constant except near the top, where it increases by almost an order of magnitude, possibly due to entrainment effects. Furthermore, $\lambda_{v_H^2}$ is always greater than λ_{w^2}, but is less than $\lambda_{c_i^2}$ for $z_* > 0.1$.

Carruthers and Hunt (1986) have shown theoretically that near the top of the boundary layer λ_w and λ_{vH} depend upon the stability of the overlying layer. They present their results in terms of integral scales normalized by a longitudinal integral scale characteristic of the middle of the boundary layer ($\lambda_H \approx 0.5z_i$) as functions of the dimensionless parameter $N\lambda_H/w_*$, where N is the Brunt–Väisälä frequency of the overlying stable layer. For the AMTEX flights, $N\lambda_H/w_* \approx 9$ with minimum and maximum values of 7 and 13, respectively. For $N\lambda_H/w_* = 9$, they predict a value of $\lambda_w/\lambda_H \approx 0.3$ and $\lambda_{vH}/\lambda_H \approx 0.8$ near the interface. We find that $\lambda_w/\lambda_H > 0.5$ and λ_{vH}/λ_H is as large as 5. However, their results apply to a shear-free case, which is not generally true for the AMTEX situation (Jensen and Lenschow, 1978).

Integral length scales for the vertical fluxes of heat, humidity, ozone, and horizontal momentum, and the covariances θq, qs, and θs follow the relations:

$$\left.\begin{aligned} \lambda_{wc_i}/z_i &= 0.16z_*^{1/3} \\ \lambda_{wv_H}/z_i &= 0.12z_*^{1/3} \\ \lambda_{c_1c_2}/z_i &= 0.4z_*^{1/2} \end{aligned}\right\} \qquad (11)$$

The flux integral scales follow the ⅓ power law dependency found by Lenschow and Stephens (1980) for the size of thermals, while the other covariance integral scales follow the same power law as the scalar variances.

The relationships for λ_{w^2}/z_i and $\lambda_{c_i^2}/z_i$ versus z_* differ from the relationships that have been measured for the wavelengths of their respective spectral peaks (actually peaks in the spectra multiplied by wavenumber). This implies that their spectral shapes are also a function of z_*, and that the ratio of integral scale to spectral peak wavelength can be used to specify spectral shape. This variation with z_* is particularly evident for λ_{w^2}/z_i. Kaimal et al. (1976) showed that the relation

$$\Lambda_w = \begin{cases} 5.9z, & z \leqslant 0.1z_i \\ 1.5z_i(1 - e^{-5z_*}), & 0.1z_i < z < z_i \end{cases} \qquad (12)$$

is a good fit to the wavelength of the spectral peak for w, denoted by Λ_w, for data obtained over land from a tethered balloon. LeMone (1978) found that the cross-wind Λ_w measured from an aircraft in the slightly unstable marine boundary layer also follows this relation.

Unauthenticated | Downloaded 10/05/24 05:53 AM UTC

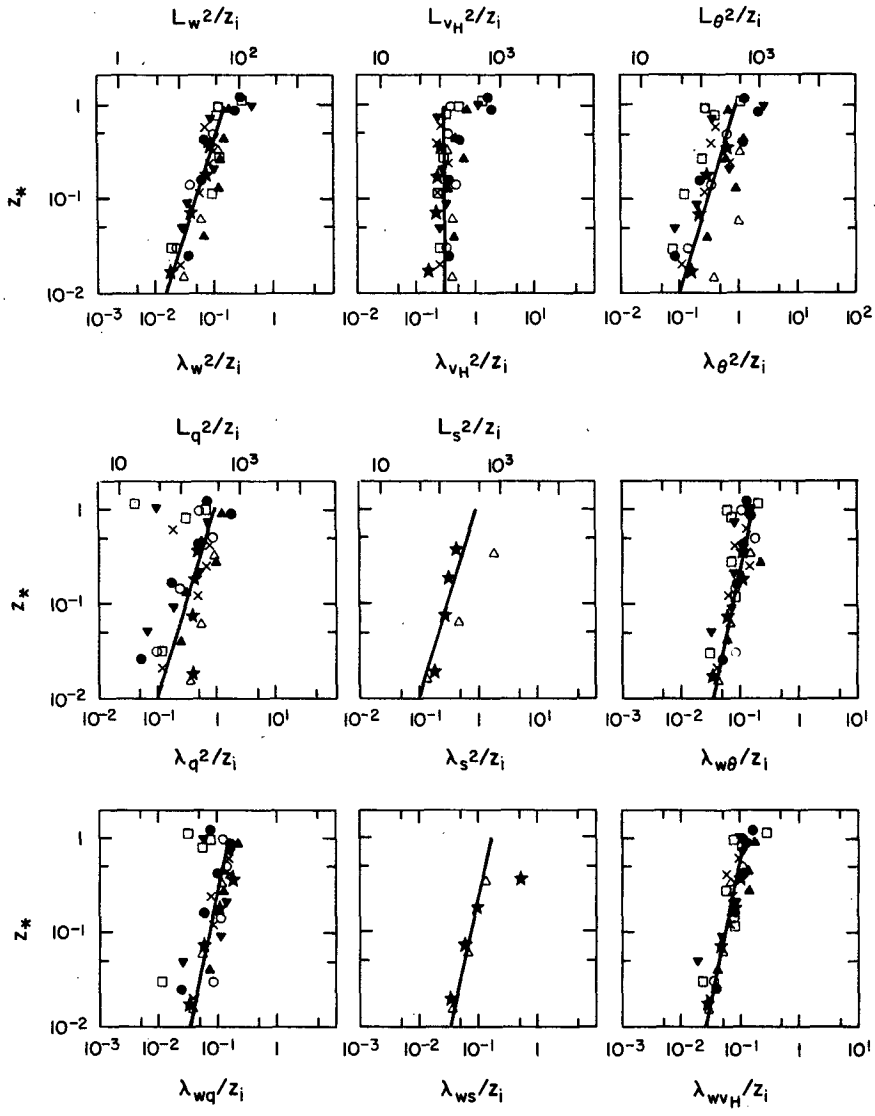

FIG. 4. Integral scales (bottom scales) and averaging lengths for 10% accuracy (top scales) for variances, and integral scales for covariances as a function of normalized height.

We have found that this relation also fits the AMTEX vertical velocity spectra. On the other hand, Caughey and Palmer (1979) obtained a somewhat different empirical relationship. They found, based on more detailed measurements near z_i, that in the upper 20% of the convective boundary layer, Λ_w decreased to about 10% to 20% of its maximum value, which they estimate to be about $1.6z_i$ at $z_* \approx 0.6$. Carruthers and Hunt (1986), however, show that in the upper part of the boundary layer, Λ_w is related to the stability of the overlying stably-stratified layer. Furthermore, Jensen and Lenschow (1978) have found that two spectral peaks may be present in the vertical velocity spectra measured at z_i. Therefore, we choose to use the relation of Kaimal et al. (1976), with the caution that it is probably not very accurate near z_i. The ratio λ_w/Λ_w, using (12) for Λ_w and (10), divided by 0.67 (to obtain λ_w from λ_{w2}) for λ_w is plotted in Fig. 6.

Kristensen et al. (1983) have developed a kinematic model of turbulence from which the ratio λ_w/Λ_w can be computed as a function of the parameter μ_3, for the vertical velocity spectrum

$$F_w(k) = Ak_3^{-5/3} \frac{3 + 8(k/k_3)^{2\mu_3}}{[1 + (k/k_3)^{2\mu_3}]^{(5/6\mu_3)+1}} \qquad (13)$$

where k is wavenumber, k_3 is the wavenumber that specifies the location of the spectral roll-off, and A is a constant proportional to the variance of w. This spectrum can be considered a generalization of the von Kármán spectrum (von Kármán, 1948), in which, for isotropic turbulence, $\mu_3 = 1$. The parameter μ_3 specifies

Unauthenticated | Downloaded 10/05/24 05:53 AM UTC

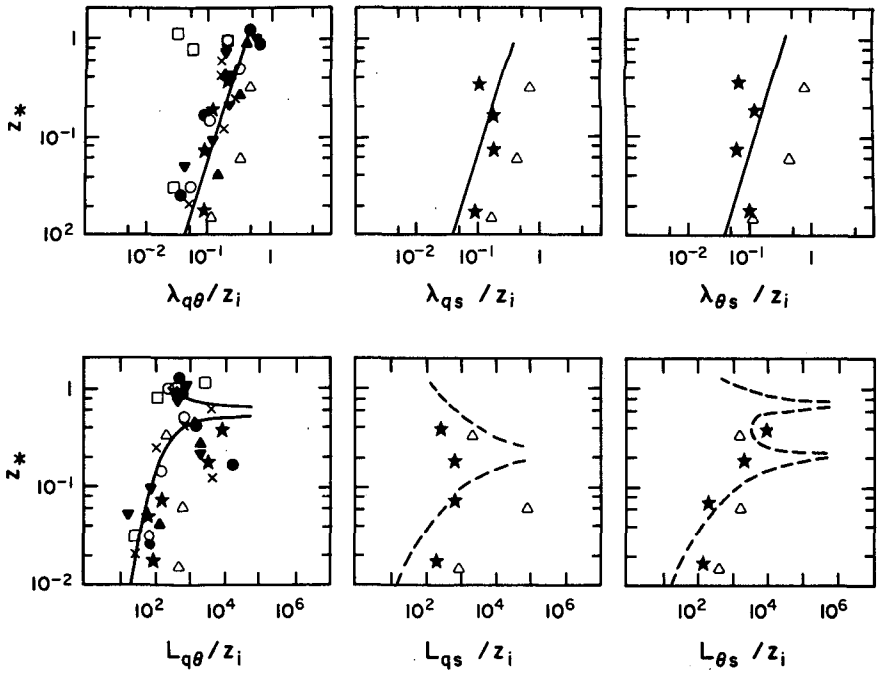

FIG. 5. Integral scales (top) and averaging lengths for 10% accuracy (bottom) for covariances as a function of normalized height.

the sharpness of the spectral knee, where the spectrum goes through a transition from zero slope to $-5/3$ slope. The functional relationship between λ_w/Λ_w and μ_3 for the spectrum given by (13) is plotted in Fig. 7. Combining this with the observed ratio of λ_w/Λ_w versus z_*, we can calculate the variation of μ_3 with z_*, which is plotted in Fig. 6. We see that the sharpness of the spectral knee reaches a maximum at $z_* \approx 0.25$. This is likely due to the effects of thermals, which have a preferred size and are most clearly defined in this middle region of the boundary layer (Lenschow and Stephens, 1980).

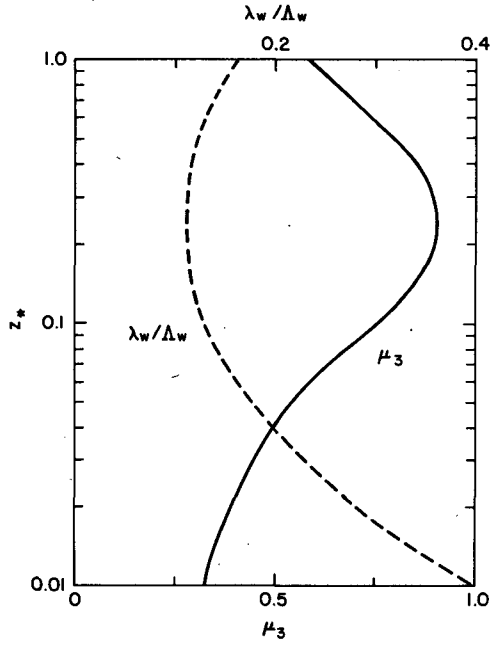

FIG. 6. Ratio of the vertical velocity spectral peak to the integral scale Λ_w/λ_w, and the spectral "sharpness parameter" for vertical velocity μ_3 as functions of normalized height.

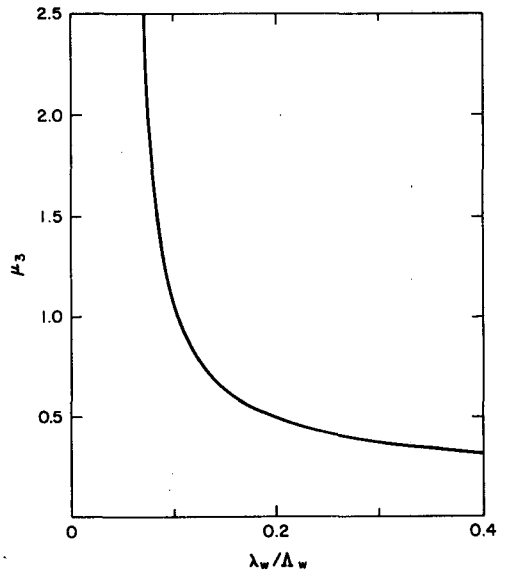

FIG. 7. Ratio of the vertical velocity spectral peak top the integral scale as a function of the spectral "sharpness parameter."

Unauthenticated | Downloaded 10/05/24 05:53 AM UTC

b. Averaging lengths for second-order moments

The length over which to average the aircraft data for calculating variances is obtained from (8). Since the kurtosis for most of the variables was found to be close to the Gaussian value of three throughout most of the boundary layer, we take it to be three for all variables. Therefore, the averaging lengths for variances differ only by a constant from the integral scales, and the integral length scale curves can be scaled to give the averaging length for a particular value of a. In fact, the kurtosis for w approaches four near the surface and near the top of the boundary layer, but is closer to three in the middle, while the kurtoses for θ and q, although quite scattered, average closer to four throughout the boundary layer. The top scales for the variances in Fig. 4 are the averaging lengths for a measurement accuracy of $a = 0.1$; the averaging lengths for variance are also specified by (10), except that the constants are multiplied by 400:

$$\left.\begin{aligned} L_{w^2}/z_i &= 64z_*^{1/2} \\ L_{v_H^2}/z_i &= 120 \\ L_{c_i^3}/z_i &= 400z_*^{1/2} \end{aligned}\right\}. \tag{14}$$

Figures 5 and 8 show the averaging lengths for the vertical fluxes and scalar covariances, calculated from (7). We can also calculate expressions for the averaging lengths from empirical expressions for the second moment terms obtained in previous investigations and substituted into (7). These expressions are also plotted in Figs. 5 and 8. The curve for averaging length for temperature flux in Fig. 8 is obtained from the empirical formulations of Lenschow et al. (1980): $\langle w'^2\rangle/w_*^2 = 1.8z_*^{2/3}(1 - 0.8z_*)^2$, $\langle\theta'^2\rangle/\theta_*^2 = 1.8z_*^{-2/3}$, and $\langle w'\theta'\rangle/(w_*\theta_*) = 1 - 1.2z_*$; and the formulation for $\lambda_{w\theta}/z_i$ given by (11):

$$L_{w\theta}/z_i = 32z_*^{1/2}\left[3.2\left(\frac{1 - 0.8z_*}{1 - 1.2z_*}\right)^2 + 1\right]. \tag{15}$$

This curve is a reasonable fit to the observed points, although it is not applicable to the region $z_* > 0.8$ for the cases considered here, since $\langle\theta'^2\rangle/\theta_*^2$ is larger there than predicted by the above relation because of entrainment.

Similarly, L_{wq}/z_i can be calculated from the additional relations (Lenschow et al., 1980 and Wyngaard et al., 1978): $\langle q'^2\rangle/q_*^2 = 1.8z_*^{-2/3}(1 + 2z_*)^3$ and $\langle w'q'\rangle/(w_*q_*) = 1 - 0.5z_*$; and (11):

$$L_{wq}/z_i = 32z_*^{1/3}\left[3.2\left(\frac{1 - 0.8z_*}{1 - 0.5z_*}\right)^2(1 + 2z_*)^3 + 1\right]. \tag{16}$$

The factor $(1 + 2z_*)^3$ is included in the expression for $\langle q'^2\rangle/q_*^2$ to make an empirical correction, on the average, for the effects of entrainment through the top of the boundary layer, and has no theoretical justification. Furthermore, the normalized humidity flux formulation is not universal, but only represents a reasonable fit to the data presented here. Its slope depends upon the entrainment rate and the difference in humidity across the top of the capping inversion. The resulting curve agrees well with the observed values, except at the boundary layer top.

For practical applications, the function

$$L_{wc_i}/z_i = 430z_*^{2/3} \tag{17}$$

is a reasonably good fit to both (15) and (16), particularly for $z_* < 0.7$.

The averaging length for ozone flux is somewhat larger than for temperature and humidity flux. We do not, however, have sufficient observations to accurately assess the difference. Furthermore, the ozone variance contains instrument noise, which was not removed. The noise decreases r_{ws}, which increases L_{ws}. However, another reason for increased averaging length for ozone is that its boundary-layer flux is mainly a result of entrainment through the top of the boundary layer; i.e., its surface flux is considerably less than the flux at the top. In contrast, both temperature and humidity have surface fluxes that are larger in magnitude than their fluxes at the top. Moeng and Wyngaard (1984) have shown, through numerical simulation, that a scalar flux at the surface generates variance more efficiently than a flux at the top. As an example, to demonstrate the effect of this difference, we compare the limiting cases of the averaging length resulting from a scalar diffusing upwards from the surface with zero flux at the top with

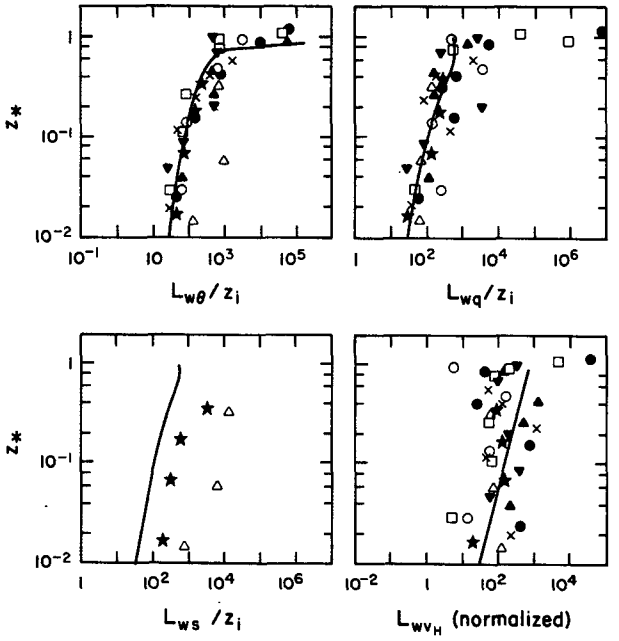

FIG. 8. Averaging lengths for 10% accuracy for vertical fluxes. Formulations for the curves are given in the text.

Unauthenticated | Downloaded 10/05/24 05:53 AM UTC

that obtained from a scalar diffusing downwards from the top with zero flux at the surface. Moeng and Wyngaard (1984) obtained the following expressions for the normalized scalar variance generated solely by a flux at the surface with a linear decrease to zero flux at the top (denoted by a subscript b), and the scalar variance generated solely by a flux at the top with a linear decrease to zero flux at the bottom (denoted by a subscript t):

$$\frac{\langle s_b'^2\rangle w_*^2}{\langle w's_b'\rangle_0^2} = r_{ws^b}^{-2}\frac{\langle w'^2\rangle\langle w's_b'\rangle_0}{w_*^2\langle w's_b'\rangle} = 0.47z_*^{-5/4}$$

$$\frac{\langle s_t'^2\rangle w_*^2}{\langle w's_t'\rangle_1^2} = r_{ws^t}^{-2}\frac{\langle w'^2\rangle\langle w's_t'\rangle_1}{w_*^2\langle w's_t'\rangle} = 2.1(1-z_*)^{-3/2} \quad (18)$$

where $\langle w's_b'\rangle_0$ is the surface flux for bottom-up diffusion and $\langle w's_t'\rangle_1$ is the flux at the top for top-down diffusion. Substituting $\langle w'^2\rangle/w_*^2 = 1.8z_*^{2/3}(1-0.8z_*)^2$ (Lenschow et al., 1980) and the linear flux variations with height into (17), then substituting both expressions given in (17) into (7), and taking the ratio of the averaging length for top-down diffusion to that for bottom-up diffusion (with the assumption that the integral length scales are the same for both), we have

$$\frac{L_{ws_t}}{L_{ws_b}} = \frac{3.8z_*^{-1/3}(1-z_*)^{-3/2}(1-0.8z_*)^2+1}{0.85z_*^{-7/12}(1-0.8z_*)^2(1-z_*)^{-1}+1}. \quad (19)$$

This function is plotted in Fig. 9. We see that because of the smaller correlation coefficient for top-down compared to bottom-up diffusion, through most of the mixed layer $L_{ws_t} \approx 3L_{ws_b}$.

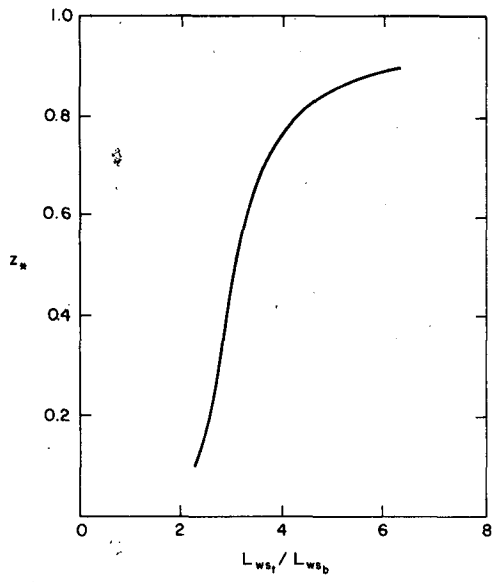

FIG. 9. Ratio of the averaging length for a scalar flux induced by top-down diffusion to that induced by bottom-up diffusion. The normalization factor for the momentum flux averaging length is given in (24).

A curve for the $q\theta$ covariance was calculated from the empirical observations presented by Wyngaard et al. (1978). The curve $r_{q\theta} = 0.8 - 1.4z_*$ fits their data well. Substituting this, along with (11) into (7), we have

$$L_{q\theta}/z_i = 80z_*^{1/2}[(0.8-1.4z_*)^{-2}+1], \quad (20)$$

which is also plotted in Fig. 5. A schematic curve for L_{qs}/z_i is sketched in Fig. 5 based on the observation that q and s are negatively correlated up to $z_* = 0.2$ to 0.3, then positively correlated above this level. This is because the surface is a source for humidity and a sink for ozone, while entrainment generates a positive flux in both species in the upper part of the boundary layer. The ozone flux becomes positive at $z_* = 0.2$ to 0.3, which means that the qs correlation should pass through zero, and therefore L_{qs}/z_i becomes infinite close to this level. The curve for $L_{\theta s}/z_i$ becomes infinite at two levels since θ and s are negatively correlated up to $z_* = 0.2$ to 0.3, then positively correlated up to $z_* = 0.7$ to 0.8, then negatively correlated above this level. This is because the ground is a heat source and an ozone sink, but the ozone flux becomes positive around $z_* = 0.2$ to 0.3, then the temperature flux becomes negative around $z_* = 0.7$ to 0.8. At each of these zero crossings, $L_{\theta s}/z_i$ becomes infinite.

The momentum flux averaging length cannot be so simply normalized by mixed layer variables. As Wyngaard (1985) has pointed out, the momentum flux scales with u_* (here we define the momentum flux as the square root of the sum of the squares of the two horizontal momentum flux components), while the velocity variances scale with w_* (Lenschow et al., 1980); that is, $\langle v_H'w'\rangle/u_*^2$, $\langle v_H'^2\rangle/w_*^2$, and $\langle w'^2\rangle/w_*^2$ are functions only of z_*. Assuming that $\langle v_H'^2w'^2\rangle$ has a Gaussian distribution, we have

$$\langle v_H'^2w'^2\rangle = \langle v_H'^2\rangle\langle w'^2\rangle + 2\langle v_H'w'\rangle^2. \quad (21)$$

Substituting (21) into (6),

$$L_{wv_H}/z_i = 2\left(1+\frac{\langle v_H'^2\rangle\langle w'^2\rangle}{\langle v_H'w'\rangle^2}\right)\frac{\lambda_{wv_H}}{a^2}. \quad (22)$$

We let

$$f(z_*) = \frac{\langle v_H'^2\rangle\langle w'^2\rangle u_*^4}{2\langle v_H'w'\rangle^2 w_*^4\kappa^{4/3}}$$

where κ is von Kármán's constant. Since $w_*^4/u_*^4 = (-z_i/\kappa L)^{4/3}$, where L is the Monin–Obukhov length, we have

$$L_{wv_H} = 2[1+0.5f(z_*)(-z_i/L)^{4/3}]\lambda_{uw}/a^2. \quad (23)$$

Therefore,

$$\frac{L_{wv_H}-2\lambda_{wv_H}/a^2}{z_i(-z_i/L)^{4/3}} = \frac{f(z_*)\lambda_{wv_H}}{z_ia^2}. \quad (24)$$

This normalized averaging length, which is now only a function of z_*, is plotted in Fig. 8. The relation

$$\frac{L_{wv_H}-2\lambda_{wv_H}a^{-2}}{z_i(-z_i/L)^{4/3}} = 220z_*^{1/3} \quad (25)$$

Unauthenticated | Downloaded 10/05/24 05:53 AM UTC

is a reasonably good fit to the observations, although the scatter is large enough that the power law coefficient cannot be accurately estimated. We compared the scatter around a least-squares-fit line to the points in Fig. 8 to the scatter around a least-squares-fit line to the points L_{wvH}/z_i, and found that the normalization used in (25) results in considerably less scatter than for L_{wvH}/z_i. Substituting (11) into (25), and solving for L_{wvH}/z_i, we have

$$L_{wvH}/z_i = z_*^{1/3}[220(-z_i/L)^{4/3} + 0.24a^{-2}]. \quad (26)$$

We see that for $a \geq 0.10$ and $-z_i/L > 1$, the second term in (26) is <11% of the first. Thus, in almost all situations,

$$L_{wvH}/z_i = 220z_*^{1/3}(-z_i/L)^{4/3}. \quad (27)$$

We note that L_{wvH}/z_i is everywhere greater than the normalized averaging length for scalar fluxes whenever $-z_i/L > 1.7$, and since $-z_i/L \gg 1$ in a convective boundary layer, $L_{wvH}/z_i \gg L_{wci}/z_i$.

We can calculate the actual relative error for a particular measurement leg from (4),

$$a = \sigma_f/\langle f\rangle = \left(\frac{2\langle f'^2\rangle\lambda_f}{L_f'\langle f\rangle^2}\right)^{1/2} \quad (28)$$

where L_f' is now the length of the actual measurement leg. Figure 10 shows a plot of momentum flux, scaled by the surface friction velocity, along with the scaled temperature and humidity fluxes with the error bars for a relative error of 10%. For the momentum flux the error bars are about equal to the flux, and the flux

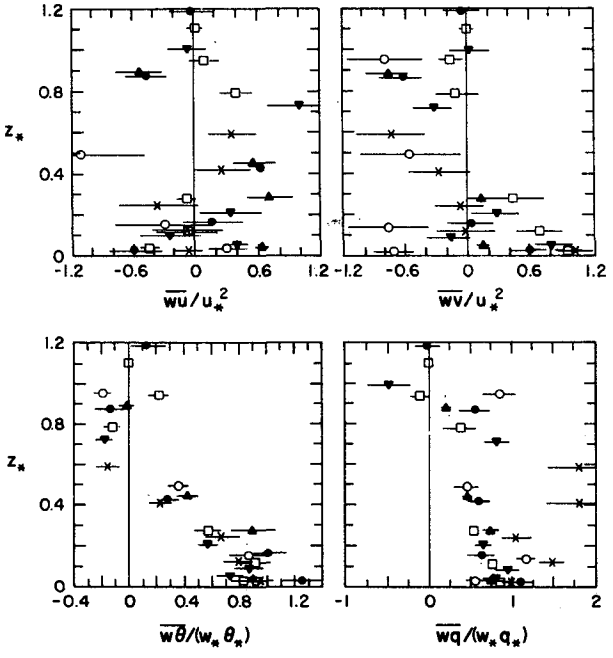

FIG. 10. Expected errors (denoted by the horizontal lines) for the measured vertical fluxes.

measurements are scattered. From Fig. 8, we see that the averaging length necessary to measure flux to 10% accuracy for $-z_i/L = 20$ (about the average for the set of legs used here) is about 10^4 km. This is about 100 times the average length of the legs used in Fig. 10, which is in good agreement with the calculated relative error. For the vertical fluxes of temperature and moisture, the error bars are about 20% and we see that the data available are sufficient to obtain a reasonably good picture of the flux profiles.

6. Concluding remarks

We have used aircraft measurements in the convective boundary layer over both water and land surfaces to calculate integral and averaging length scales of second-order moment quantities. In order to measure variances to about 10% accuracy, the averaging length needs to be from 50 to 400 times the height of the boundary layer (14). For scalar fluxes, the averaging length needs to be from 100 to 500 times the height of the boundary layer (17). For momentum flux, the picture is more complicated, since the averaging length is stability dependent. Typically, an averaging length of greater than 5×10^3 times the boundary layer height is required (27). Obviously, this seriously limits the accuracy that is possible to achieve from towers or aircraft measurements, since the time required for an aircraft to fly this distance is at least half a day.

Because of this limitation, it is desirable to investigate alternative techniques for measuring momentum flux. Wyngaard (1985) points out that area-averaging techniques may very well be a feasible alternative, since $L_{wuH}/\lambda_{wuH} = 2000$ for linear averaging, while area averaging gives a ratio of $L_{wuH}/\lambda_{wuH} = (2000)^{1/2} \approx 45$; i.e., an area 45 integral scales on a side, which is on the order of 5 km. Eymard (1984), for example, presents dual Doppler radar measurements of area-averaged momentum flux over a rectangle 20 km by 15 km in a boundary layer with convective clouds. Kropfli (1986) discusses the use of a single Doppler radar for this type of measurement.

Acknowledgments. The data were obtained from flights carred out by the NCAR Research Aviation Facility. We are grateful for useful discussions with S. Clifford, J. C. Wyngaard, J. R. Herring and Chin-Hoh Moeng. We thank Ginger Caldwell for her help in developing and explaining to us the proper use of statistical confidence limits and significance levels. Finally we are indebted to Leif Kristensen who provided encouragement and many helpful comments on the manuscript, and developed the model presented in Appendix B.

APPENDIX A

Estimating Integral Scales

The power spectrum $S(k)$ and the autocovariance function $R(r)$ are related by the transforms

Unauthenticated | Downloaded 10/05/24 05:53 AM UTC

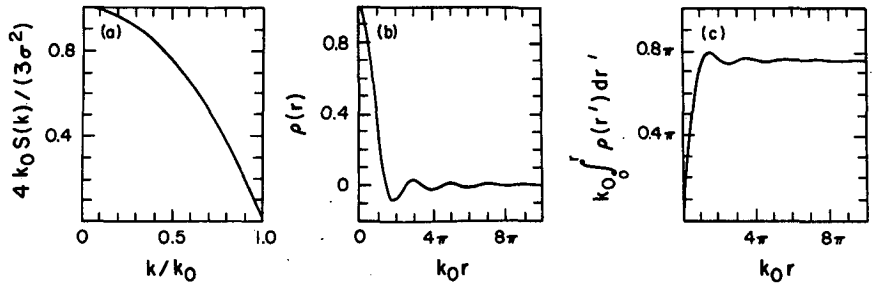

FIG. A1. Power spectrum given by $\frac{4k_0S(k)}{3\sigma^2}[1-(k/k_0)^2]$, this autocorrelation coefficient and the normalized integral of the autocorrelation coefficient.

$$S(k) = \frac{1}{\pi}\int_0^\infty R(r)\cos krdr$$

$$R(r) = 2\int_0^\infty S(k)\cos krdk. \tag{A1}$$

At $k = 0$, the power spectrum becomes

$$S(0) = \frac{1}{\pi}\int_0^\infty R(r)dr. \tag{A2}$$

Therefore, the integral scale (2) can be written as

$$\lambda = \pi S(0)/\sigma^2 \tag{A3}$$

where $\sigma^2 = R(0)$. Thus the integral scale can be obtained either from (2) or (A3).

Compte-Bellot and Corrsin (1971) note that measured integral scales are only "simple extrapolations" of partially measured $R(r)$ or $S(k)$, and that these extrapolations should correspond to a mathematically possible flow field identical to the real flow field at moderate and large wavenumbers (or frequencies) corresponding to the conditions of the experiment. The authors suggest that, for isotropic turbulence, the power spectrum of the longitudinal velocity component at small wavenumbers can be characterized by a downward parabola with zero slope at $k = 0$. To test the accuracy of the method used here to determine the integral scales, we used a parabola of the form

$$S(k) = \frac{3\sigma^2}{4k_0}\left[1-\left(\frac{k}{k_0}\right)^2\right] \tag{A4}$$

where k_0 is the cutoff wavenumber. The autocovariance function of this power spectrum is

$$R(r) = 3\left(\frac{\sigma}{k_0r}\right)^2\left(\frac{\sin k_0r}{k_0r} - \cos k_0r\right). \tag{A5}$$

The normalized power spectrum, the autocorrelation coefficient $\rho(r) = R(r)/R(0)$, and $F(r) = k_0\int_0^\infty \rho(r')dr'$ are plotted in Fig. A1. We see that the shape of the autocorrelation function is similar to that in Fig. 1. The normalized integral scale, $\lambda k_0 = k_0\int_0^\infty \rho(r)dr = \pi S(0)/\sigma^2 = 3\pi/4 = 2.356$. Our procedure is to estimate the integral scale as the value of $F(r)$ at its first maximum. For the autocorrelation function used here, this value is 2.483. Thus, our procedure overestimates the actual integral scale in this case by about 5%. This is probably typical of the effect of our procedure in applying it to the actual aircraft data; i.e., by selecting the value of $F(r)$ at its first maximum, we obtain a somewhat larger value for the integral scale than what other procedures might give. We have also plotted in Fig. 1 the power spectrum given by (A4) using the integral scale obtained from the maximum of $\int_0^r \rho(r')dr'$, which is also plotted in Fig. 1. The model spectrum fits the observed spectrum well in the region where the spectral peak occurs.

APPENDIX B

The Ratio of Integral Scales of a Variable to Its Variance in the Inertial Subrange

Assume that for the process α, $\langle\alpha\rangle = 0$. Its autocorrelation function is

$$\rho_\alpha(r) = \frac{\langle\alpha(x)\alpha(x+r)\rangle}{\sigma_\alpha{}^2}. \tag{B1}$$

We also define a process $\beta = \alpha^2$, which has $\langle\beta\rangle = \sigma_\alpha{}^2$, and

$$\rho_\beta(r) = \frac{\langle[\beta(x)-\beta\rangle][\beta(x+r)-\langle\beta\rangle]}{\sigma_\beta{}^2} \tag{B2}$$

$$= \frac{\langle\beta(x)\beta(x+r)\rangle - \sigma_\alpha{}^4}{\sigma_\beta{}^4}. \tag{B3}$$

For a Gaussian process, $\langle\beta(x)\beta(x+r)\rangle = \sigma_\alpha{}^4 + 2\rho_\alpha{}^2(r)\sigma_\alpha{}^4$. Therefore, (B3) becomes

$$\rho_\beta(r) = \frac{\sigma_\alpha{}^4 + 2\rho_\alpha{}^2(r)\sigma_\alpha{}^4 - \sigma_\alpha{}^4}{2\sigma_\alpha{}^4} = \rho_\alpha{}^2(r). \tag{B4}$$

The autocorrelation function for small values of r can be expressed as (e.g., Tatarskii, 1961), $\rho_\alpha(r) = 1 - (k_0r)^{2/3}$, where k_0 is some constant wavenumber. For simplicity, we assume that this simple formulation applies to the longitudinal velocity component out to $\rho_\alpha(r) = 0$; i.e.,

Unauthenticated | Downloaded 10/05/24 05:53 AM UTC

$$\rho_\alpha(r) = \begin{cases} 1 - (k_0 r)^{2/3}, & r \leq k_0^{-1} \\ 0, & r > k_0^{-1}. \end{cases}$$

Integrating $\rho_\alpha(r)$ and $\rho_\alpha{}^2(r)$ to the zero crossing, which is equivalent to the process used here of integrating out to the maximum of $F(r) = \int_0^r \rho(r')dr'$, we have

$$\lambda_\alpha = \int_0^{k_0^{-1}} \rho_\alpha(r)dr = \frac{2}{5} k_0^{-1}$$
$$\lambda_\alpha{}^2 = \int_0^{k_0^{-1}} \rho_{\alpha^2}(r)dr = \frac{8}{35} k_0^{-1}. \tag{B5}$$

The ratio of these integral scales is $\lambda_{\alpha^2}/\lambda_\alpha = 0.57$.

REFERENCES

Batchelor, G. K., 1953: *Homogeneous Turbulence,* Cambridge University Press, 208 pp.

Carruthers, D. J., and J. C. R. Hunt, 1986: Velocity fluctuations near an interface between a turbulent region and a stably stratified layer. *J. Fluid Mech.* (in press).

Caughey, S. J., and S. G. Palmer, 1979: Some aspects of turbulence structure through the depth of the convective boundary layer. *Quart. J. Roy. Meteor. Soc.,* **105,** 811–827.

Compte-Bellot, G., and S. Corrsin, 1971: Simple Eulerian time correlation of full- and narrow-band velocity signals in grid-generated, 'isotropic' turbulence. *J. Fluid Mech.,* **48**(Part 2), 273–337.

Eymard, L., 1984: Radar analysis of atropical convective boundary layer with shallow cumulus clouds. *J. Atmos. Sci.,* **41,** 1380–1393.

Jensen, N. O., and D. H. Lenschow, 1978: An observational investigation of penetrative convection. *J. Atmos. Sci.,* **35,** 1924–1933.

Kaimal, J. C., J. C. Wyngaard, D. A. Haugen, O. R. Cote, Y. Izumi, S. J. Caughey and C. J. Readings, 1976: Turbulence structure in the convective boundary layer. *J. Atmos. Sci.,* **33,** 2152–2169.

von Kármán, T., 1948: Progress in the statistical theory of turbulence. *Proc. Natl. Acad. Sci. USA,* **34,** 530–539.

Kristensen, L., P. Kirkegaard and D. H. Lenschow, 1983: Squashed atmospheric turbulence. Risø-R-478. Risø National Laboratory, Denmark, 79 pp.

Kropfli, R. A., 1986: The use of pulsed-Doppler radar in studies of the planetary boundary layer. *Probing the Atmospheric Boundary Layer,* D. H. Lenschow, Ed., Amer. Meteor. Soc., (in press).

LeMone, M. A., 1978: The marine boundary layer. *Workshop on the Planetary Boundary Layer,* J. C. Wyngaard, Ed., Boulder, Amer. Meteor. Soc., 182–231.

——, and W. T. Pennell, 1975: The relationship of trade wind cumulus distribution to subcloud layer fluxes and structure. *Mon. Wea. Rev.,* **104,** 524–539.

Lenschow, D. H., and E. M. Agee, 1976: Preliminary results from the air mass transformation experiment (AMTEX). *Bull. Amer. Meteor. Soc.,* **57,** 1346–1355.

——, and P. L. Stephens, 1980: The role of thermals in the convective boundary layer. *Bound. Layer Meteor.,* **19,** 509–532.

——, J. C. Wyngaard and W. T. Pennell, 1980: Mean-field and second-moment budgets in a baroclinic, convective boundary layer. *J. Atmos. Sci.,* **37,** 1313–1326.

——, R. Pearson, Jr. and B. B. Stankov, 1981: Estimating the ozone budget in the boundary layer by use of aircraft measurements of ozone eddy flux and mean concentration. *J. Geophys. Res.,* **86,** 7291–7297.

——, —— and ——, 1982: Measurements of ozone vertical flux to oceans and forest. *J. Geophys. Res.,* **87,** 8833–8837.

Lumley, J. L., and H. A. Panofsky, 1964: *The Structure of Atmospheric Turbulence,* Interscience, 239 pp.

Moeng, C.-H., and J. C. Wyngaard, 1984: Statistics of conservative scalars in the convective boundary layer. *J. Atmos. Sci.,* **41,** 3161–3169.

Panofsky, H. A., and J. A. Dutton, 1984: *Atmospheric Turbulence,* Wiley and Sons, 397 pp.

Tatarskii, V. I., 1961: *Wave Propagation in a Turbulent Medium,* McGraw-Hill, 285 pp.

Wyngaard, J. C., 1973: On surface-layer turbulence. *Workshop on Micrometeorology,* D. A. Haugen, Ed., Boston, Amer. Meteor. Soc., 101–149.

——, 1983a: Lectures on the planetary boundary layer. *Mesoscale Meteorology—Theories, Observations, and Models,* T. Gal-Chen and D. K. Lilly, Eds., Reidel, 603–650.

——, 1983b: *Boundary-layer modeling, in Atmospheric Turbulence and Air Pollution Modelling,* F. T. M. Nieuwstadt and H. van Dop, Eds., Reidel, 69–106.

——, 1985: Measurement Physics. *Probing the Atmospheric Boundary Layer,* D. Lenschow, Ed., Amer. Meteor. Soc., (in press).

——, W. T. Pennell, D. H. Lenschow and M. A. LeMone, 1978: The temperature-humidity covariance budget in the convective boundary layer. *J. Atmos. Sci.,* **35,** 47–58.

Unauthenticated | Downloaded 10/05/24 05:53 AM UTC